Original Article

Tumor Biology

Tumor Biology
March 2017: 1–12

DOI: 10.1177/1010428317695943
journals.sagepub.com/home/tub
SAGE

Prostate-specific membrane antigen–directed nanoparticle targeting for extreme nearfield ablation of prostate cancer cells

Seung S Lee[1,2], Philip JR Roche[1], Paresa N Giannopoulos[1], Elliot J Mitmaker[1,3], Michael Tamilia[4], Miltiadis Paliouras[1,2] and Mark A Trifiro[1,2,4]

Abstract

Almost all biological therapeutic interventions cannot overcome neoplastic heterogeneity. Physical ablation therapy is immune to tumor heterogeneity, but nearby tissue damage is the limiting factor in delivering lethal doses. Multi-walled carbon nanotubes offer a number of unique properties: chemical stability, photonic properties including efficient light absorption, thermal conductivity, and extensive surface area availability for covalent chemical ligation. When combined together with a targeting moiety such as an antibody or small molecule, one can deliver highly localized temperature increases and cause extensive cellular damage. We have functionalized multi-walled carbon nanotubes by conjugating an antibody against prostate-specific membrane antigen. In our in vitro studies using prostate-specific membrane antigen–positive LNCaP prostate cancer cells, we have effectively demonstrated cell ablation of >80% with a single 30-s exposure to a 2.7-W, 532-nm laser for the first time without bulk heating. We also confirmed the specificity and selectivity of prostate-specific membrane antigen targeting by assessing prostate-specific membrane antigen–null PC3 cell lines under the same conditions (<10% cell ablation). This suggests that we can achieve an extreme nearfield cell ablation effect, thus restricting potential tissue damage when transferred to in vivo clinical applications. Developing this new platform will introduce novel approaches toward current therapeutic modalities and will usher in a new age of effective cancer treatment squarely addressing tumoral heterogeneity.

Keywords

Prostate-specific membrane antigen, multi-walled carbon nanotubes, therapeutics, photothermal cell ablation, prostate cancer

Date received: 25 September 2016; accepted: 23 December 2016

Introduction

Prostate cancer (CaP) is the most common neoplastic disorder in men, but only a fraction of those affected, whom cannot yet be identified, will develop more significant advanced disease. As a consequence, initial localized disease is difficult to address and is prone to over-diagnosis and over-treatment. In early disease, passive active surveillance is most likely practiced. Later-stage disease is associated with a transition of the tumor(s) toward an androgen-independent state, a fatal prognostic sign.[1] Surgery is clearly curative in early disease, but the complications are still very substantial.

[1]Segal Cancer Centre and Lady Davis Institute for Medical Research, Jewish General Hospital, Montreal, QC, Canada
[2]Division of Experimental Medicine, Department of Medicine/Oncology, McGill University, Montreal, QC, Canada
[3]Department of Surgery, McGill University, Montreal, QC, Canada
[4]Division of Endocrinology, Jewish General Hospital, Montreal, QC, Canada

Corresponding author:
Miltiadis Paliouras, Segal Cancer Centre and Lady Davis Institute for Medical Research, Jewish General Hospital, 3755 Cote-Ste-Catherine Rd., Montreal, QC H3T 1E2, Canada.
Email: miltiadis.paliouras@mcgill.ca

Early cancers evolve through many somatic mutations[2–6] and undergo many selection processes, and many times induced by classical drug therapies themselves initiating drug resistance. CaP studies have shown extensive genetic alterations exemplified by single missense mutations, copy number variation, splicing variants, genetic rearrangements, and short DNA alterations in a large number of genes.[3,7–12] However, physical agent therapies are immune to genetic alterations, as they are more likely to deliver damaging entities to a targeted "area" or "field," and as such are lethal to tumor cells irrespective of their genetic background, as long as they are present within the targeted area.

Thus, physical agents could circumvent many of the concerns of treating advanced localized disease and would be curative, where surgical options may be unavailable. Therefore, agents that manipulate temperature, light, or radioactivity should be considered. Although used in the past, they are limited by possible nearby tissue damage. There has never been an attempt to devise an adequate systematic effective targeted nearfield delivery of physical agents. These modalities, in addition to classical radiotherapy and brachytherapy, usually lack sufficient cell destruction or cause significant damage to critical nearby tissues. For example, a limitation of high-intensity focused ultrasound (HIFU) is the potential damage to nearby tissues and therefore lacks high precision, and thereby limited to CaP in situ.[13]

A superior targeting approach for cancer cells would require a mechanism by which a highly localized physical agent is in immediate proximity to the cells, ideally at the cell surface, causing significant cellular/intracellular damage with extreme efficiency deferring nearby tissue effect. To do so, we employed functionalized multi-walled carbon nanotubes (MWCNTs), which are engineered soluble colloidal suspensions possessing tunable thermal, magnetic, and electromagnetic wave interaction properties.

Several groups have used nanoparticles for ablative therapy (many without targeting it to the tumor, or using direct injection[14–17]) which was very effective yet introduced excessive bulk heating ($t > 50°C$). However, bulk heating of a treated region can cause serious nearby damage in the clinical setting. Other nanoparticles require large light fluxes/ultra-short light pulse modulations[18] with prolonged exposure of 5–15 min[19] even for moderate temperature increases of only few degrees, which can be detrimental and inefficient with lower rates of cell ablation.

Presently, a high level of biological and chemical functionalization potential is available for binding of targeting ligands to MWCNT nanoparticles, thus mediating cancer cell recognition and subsequent nearfield cell ablation. Expanding on our previous study[20] of MWCNT nanoparticle-mediated targeting strategy, here we specifically target prostate-specific membrane antigen (PSMA) expressed in CaP cells by optimizing the nanoparticle functionalization and antibody conjugation chemistry. We also aimed to show that highly efficient targeting should place a sufficient number of nanoparticles directly on the surface of cells so as to deliver exquisite extreme nearfield heat energy sufficient for cell ablation without bulk heating. Bulk heating reflects misdirected energy and can have serious effects on nearby tissue if used in vivo. These MWCNTs have the added critical benefit of simultaneously providing a self-imaging platform, so as to document and quantitate successful targeting (i.e. theranostics).

Materials and methods

Cell lines and culturing

LNCaP, PC3, and HEK293 cells lines were obtained from the American Type Culture Collection (ATCC, Rockville, MD, USA). LNCaP and PC3 cells were cultured in RPMI 1640 media supplemented with 10% fetal bovine serum (FBS) and 1% penicillin/streptomycin. Cell lines were incubated at 37°C and 5% CO_2 humidified air in plastic culture flasks. Once confluent, cells were harvested by using Versene solution (0.48 mM ethylenediaminetetraacetic acid (EDTA) in phosphate-buffered saline (PBS)) to maintain cell surface integrity and were suspended in chilled PBS in preparation for incubation with functionalized MWCNTs.

MWCNT particle functionalization and antibody conjugation chemistry

MWCNTs functionalized with a carboxylic group on the surface (MWCNT-COOH) were purchased from Cheap Tubes Inc. (Cambridgeport, VT, USA). In a stock MWCNT solution, 15 mg of MWCNTs and 200 µL of polysorbate 20 solution (TWEEN 20) were suspended in d_2H_2O to obtain a final concentration of 60 mg/L. The MWCNT solution was sonicated seven times each for 20-min durations at 4°C. During each interval, 1 mL aliquots of the stock solution were prepared to assess the solubility and dispersion of MWCNTs. To evaluate the solubility and dispersion, the aliquots were filtered with a 0.45-µm Amicon filter, and the absorbance values (measured by NanoDrop UV-Vis spectrophotometer) of the filtrate were compared to the unfiltered, sonicated stock solution. The stock solution was sonicated until the absorbance values of the stock were equal to the absorbance values of the filtrate.[21,22] Size-modified MWCNT solution was mixed with 40 µL 1-ethyl-3-(3-dimethylaminopropyl)carbodiimide (EDC), 20.9 mM; 40 µL N-hydroxysuccinimide (NHS), 34.8 mM; and 20 µL 0.2 mM heterobifunctional maleimide-PEG_{5000}-NH_2 crosslinker (Mal-PEG_{5000}-NH_2; Nanocs, New York, NY) in a final volume of 300 µL. The mixture was allowed to react in 25°C for 30 min to ensure that the coupling reaction at the amine side of the PEG crosslinker is completed with

EDC-NHS-activated COOH groups of MWCNTs. Once the reaction was completed, the protein or antibody of interest containing functional groups (sulfhydryl groups) was added to the mix and was incubated at 4°C overnight to allow the maleimide side of the crosslinker to fully react with the functional sulfhydryl groups on the protein. The final product was centrifuged at 12,000*g* at 4°C for 30 min, resuspended in PBS, and was sonicated to ensure monodispersion of the antibody-functionalized MWCNTs. UV-Vis measures of the final product were obtained to ensure that the solution's absorbance values were still larger than 0.03 units at 532 nm wavelength. Conjugation of the targeting antibody to the maleimide-PEG_{5000}-NH_2 crosslinker is outlined in Supplemental Data S1 and S2.

The same PEG functionalization protocol was performed using Cy5-PEG_{5000}-NH_2 dye (Nanocs). The following PSMA antibodies (EPR6253 and EP3253) were tested (Abcam, Toronto, Canada). Other antibodies used included mouse IgG (Millipore, Billerica, MA) and α-mouse-linked-HRP (horseradish peroxidase; GE Healthcare, Baie-d'Urfé, Canada).

Western blot analysis

PC3 and LNCaP cells were collected using 0.05% trypsin and lysed using 1× Reporter Lysis buffer. The samples were then precipitated overnight in room temperature before loading onto the gel; 20 µg of total-cleared cell lysate was loaded on an 8% SDS-PAGE (sodium dodecyl sulfate polyacrylamide gel electrophoresis) gel. Primary PSMA (EPR6253) antibody was diluted to 1:1000 and used under manufacturer's instructions (Abcam). Antibody against β-actin was used as a loading control.

Cell ablation studies

Using LNCaP, PC3, or HEK293 cell lines, ~300,000 cells suspended in 150 µL PBS were well mixed with 75 µL of functionalized MWCNTs or α-PSMA–MWCNTs. A negative control with PBS was also prepared. Each experiment was performed ≥3 times. These mixtures were incubated for 1 h at 37°C and 5% CO_2 on a rotator. After incubation, mixtures were centrifuged at 500*g* for 5 min, washed three times in PBS, and resuspended in 225 µL PBS. This washing step was repeated for a total of three times. The solution mixture was then aliquoted into 25 µL fractions in polymerase chain reaction (PCR) tubes, which were then subjected under green diode-pumped solid-state laser (DPSS laser; power at 2.7 W and laser emission at 532 nm) for 30 s. Finally, cell counts for laser-treated and laser-untreated cells were obtained using trypan blue staining under a hemocytometer. Cell ablation was calculated as follows: % Cells Ablated = (number of live cells post laser treatment/number of live cells pre laser treatment) × 100.

Live cell imaging with Cy5-crosslinked MWCNT

For Cy5 tagging of the MWCNTs, our standard conjugation method was employed, except maleimide-PEG_{5000}-NH_2 crosslinker was mixed with Cy5-PEG_{5000}-NH_2 (Nanocs) solution (0.2 mM; 4:1 maleimide crosslinker to Cy5 dye ratio) in the dark to provide fluorescence. The conjugated products were washed three times with PBS to ensure unbound Cy5-PEG_{5000}-NH_2 dye was removed. Approximately 50,000 PSMA-positive LNCaP and PSMA-null PC3 cells were seeded onto LabTek II chamber slides (purchased from Thermo Fisher Scientific, Rochester, NY, USA) in respective wells. The seeded cells were incubated overnight at 37°C and 5% CO_2. On the next day, α-PSMA–MWCNT conjugates with or without Cy5 and PBS control were incubated with the two cell lines for 1 h in identical conditions; 138 µL of 300 nM stock of 4′,6-diamidino-2-phenylindole dihydrochloride (DAPI) solution was also added for nuclear staining. After incubation was completed, the wells were washed three times with RPMI medium to remove any unbound Cy5-tagged MWCNTs. The chamber was then visualized under Leica spinning disk confocal microscope (Wetzlar, Germany).

Results

Non-targeted cell ablation studies

One of the major properties of nanoparticles including MWCNTs is the plasmonic generation of extreme heat at their surface upon exposure to light. Thus, we aimed to assess PEG-functionalized MWCNTs and their ability to ablate cells, when solely mixed together with HEK293 cells without antibody conjugation and without washing in a non-targeted experiment. MWCNTs were mixed in a 1:2 volume ratio of particles to cells, and exposed to a 2.7-W 532-nm laser for 5, 10, or 20 s (Figure 1(a)). Cell death was visualized by a simple trypan blue staining, with cells counted on a hemocytometer. Trypan blue will stain "dead" or necrotic cells blue, while live cells will not incorporate the dye and appear "white." With increasing exposure to the laser, the number of live cells drops. By 20 s, not a single live (or white) cell could be counted. Moreover, the number of "blue" or dead cells is also dramatically reduced from the starting input cell numbers, indicating that the process has resulted in a physical disruption/destruction of the cells. The reduced presence of "blue" cells together with the reduced number of total cells after 20-s laser exposure suggests that the cells are not undergoing an apoptotic programmed or necrosis cell death but rather a very physical ablative destruction by the generation of bulk heating (see below). After laser treatment, a portion of the cells were plated onto six-well plates and assessed for survival and growth after 5 days (Figure 1(b)). The 5- and 10-s laser exposure was not adequate to ablate all the cells, and a confluent lawn of cells could be observed

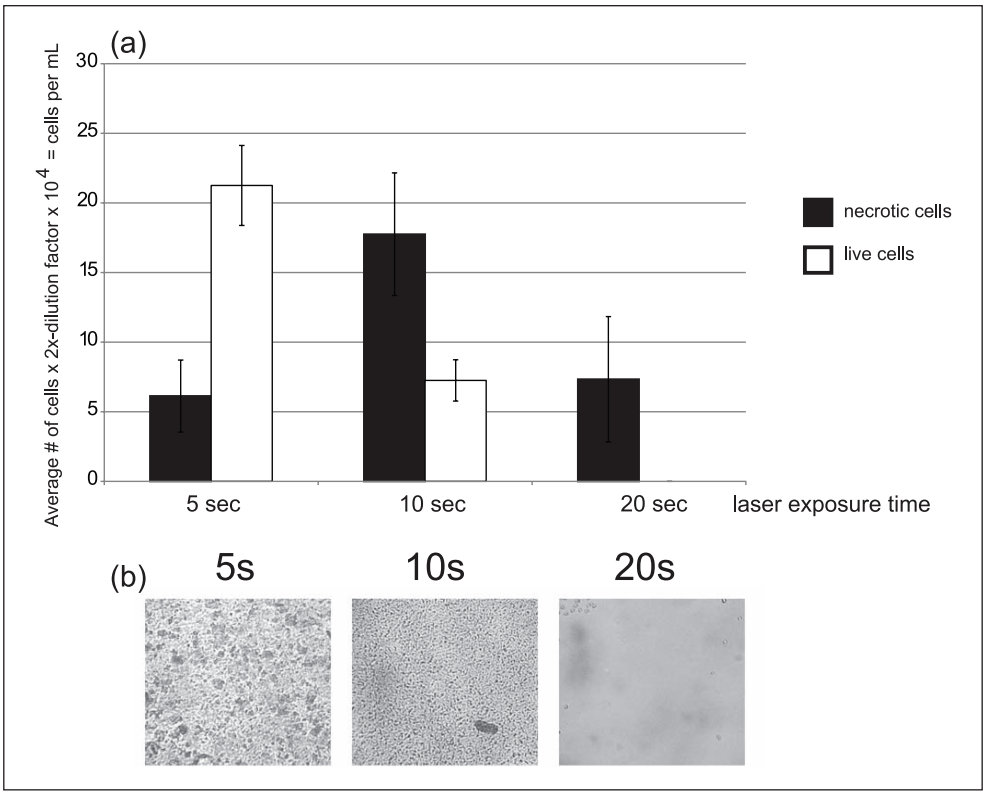

Figure 1. Non-targeted cell ablation studies. (a) PEG-maleimide-functionalized multi-walled carbon nanotubes (MWCNTs) were used to test the potential to kill HEK293 cells by bulk heating of the solution mixture and shows the effects of three different exposure times (5, 10, and 20 s) with a 2.7-W, 532-nm laser (n = 5). Following laser treatment, cells death was assessed using trypan blue staining. (b) After laser treatment, a portion of HEK293 cells were seeded into six-well plates and grown for 5 days. Following 20 s of laser treatment, no cells could be discerned growing on the plates.

after reseeding. However, from the 20-s laser treatment, we could not observe any cell growth after 5 days, emphasizing complete ablation. It is also clear that for photothermal bulk heating of MWCNTs at lower concentrations (mass per volume) of carbon-based materials are more effective compared to alternatives such as silica particles, ferrous or gold particles.[23–25]

PSMA antibody selection and nearfield targeting of LNCaP cells

To determine the effectiveness and extent of the antibody conjugation method using malemide-PEG_{5000}-NH_2 bifunctional crosslinkers, we have performed a semi-quantitative, dose-dependent chemiluminescent assay. Different amounts (2, 5, 8, 10, and 12 µg) of α-mouse HRP-IgG were conjugated onto MWCNTs as outlined in our protocol. A diluted (1:10) portion of each sample was loaded onto a microtiter plate and mixed with chemiluminescent solution. Similarly, as a standard we loaded different amounts (2, 5, 8, and 10 µg) of unconjugated α-HRP-IgG was diluted 1:1000 and each sample loaded onto a microtiter plate. Intensity of the chemiluminescent reaction is shown in Figure 2. The results display a very linear relationship on the amount of α-HRP-IgG that can be conjugated to the nanoparticles; conjugation of 12 µg α-HRP-IgG did not reach an MWCNT saturation point.

The average molecular weight of MWCNTs is in the order of 10^8 g/mol; thus, there are approximately 10^3 less particles than antibodies; each particle has approximately 10^5 COOH groups, providing a very close equimolar ration of COOH groups and antibody used in these experiments. Increasing the amount of EDC and NHS for the carbodiimide reaction to increase functionalization of the carboxylic groups on MWCNTs was ineffective, as only a marginal difference was observed, suggesting that we are employing enough carbodiimide for functionalization of the carboxylic groups (data not shown).

PSMA was selected as the target of choice for selectively targeting CaP cells. The expression of PSMA is highly restricted to human prostate secretory epithelium, its level of expression is correlated with the tumor aggressiveness, and it is present in all stages of the disease from early disease and especially elevated in advanced hormone refractory and metastatic disease.[26–29] Furthermore, PSMA provides an excellent target for monoclonal antibody strategies because it is long-lived on cancer cells and comprises a large extracellular domain. Therefore, we selected to test two different PSMA

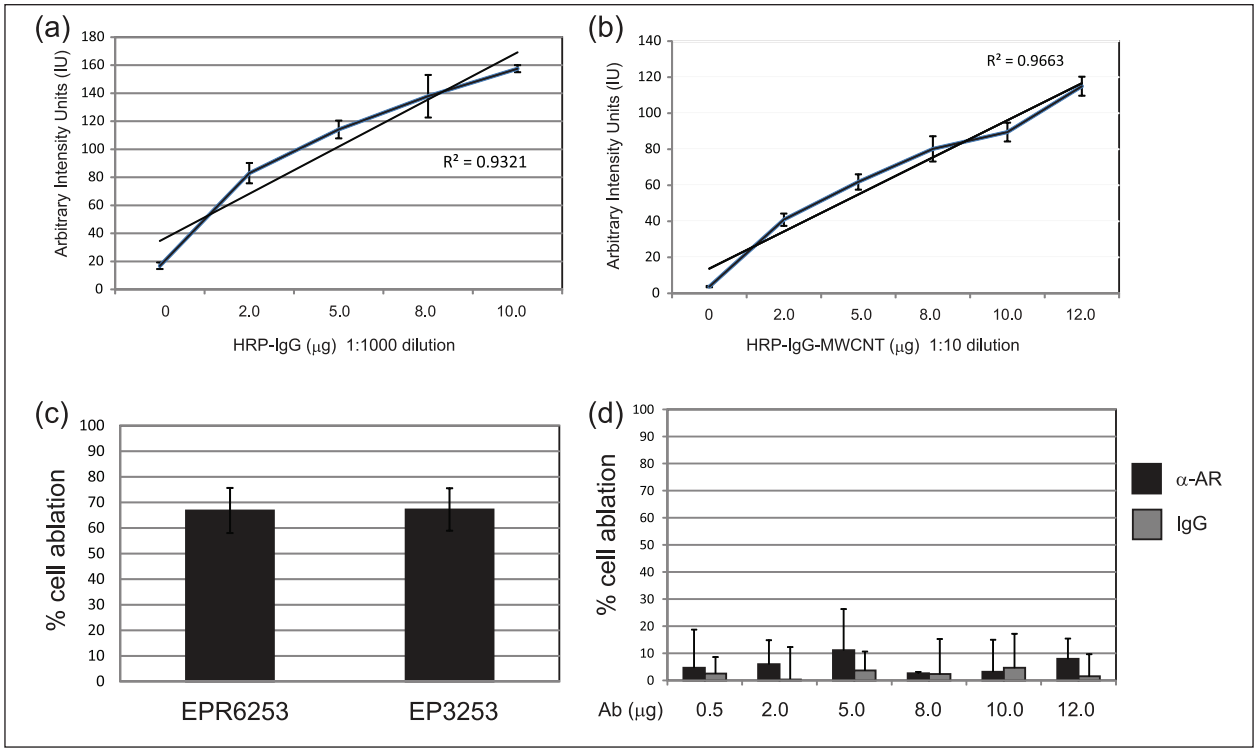

Figure 2. α-PSMA-targeted cell ablation. (a) Standard curve of HRP-IgG antibody diluted 1:1000, loaded onto a black clear bottom microplate, and mixed with chemiluminescent solution (n = 3). (b) MWCNTs conjugated with different amounts of HRP-IgG diluted 1:100, loaded onto microplate, and mixed with chemiluminescent solution (n = 3). Images were captured with a Bio-Rad gel imager, and densitometry of signal intensity was measured by ImageJ. (c) Two PSMA antibodies from Abcam (EPR6253 (n = 3) and EP3253 (n = 3)) conjugated to MWCNTs and used to ablate LNCaP cells. Both antibodies showed similar abilities to ablate cells. (d) Androgen receptor (AR; n = 3) and IgG (n = 3) antibodies were also conjugated onto MWCNTs and used as negative controls to ablate LNCaP cells.

antibodies, 5 μg of EP3253 and EPR6253 antibodies, by conjugating them onto MWCNTs and used for our targeted cell ablation studies of PSMA-expressing LNCaP cells. EP3253- and EPR6253-MWCNT conjugates were prepared and incubated in a 1:2 MWCNT:cell ratio for 1 h, washed thoroughly with PBS, and exposed to laser treatment for 30 s. Both α-PSMA–MWCNT conjugates showed efficient targeted ablation of PSMA-expressing cells, with >60% of LNCaP cells ablated (Figure 2(c)), suggesting that the difference between the two antibodies was marginal.[30]

We also assessed whether the targeting of PSMA to LNCaP is restricted to the exposed extracellular domain, and that the α-PSMA–MWCNT conjugates are not internalized. Therefore, we similarly conjugated 5 μg of the antibodies against intracellular androgen receptor (AR), which is known to be well expressed in LNCaP cells, and IgG (a non-specific targeted antibody) to MWCNTs and proceeded with cell ablation studies (Figure 2(d)). The amount of cell ablation is very minimal and significant between the α-PSMA-targeted versus α-AR- or IgG-targeted cells (EPR6253, 5 μg: α-AR $p=0.00499$, IgG $p=0.00039$; EP3253, 5 μg: α-AR $p=0.00419$, IgG $p=0.00016$), and, moreover, illustrates that the MWCNTs are not internalized to target intracellular moieties such as the AR. This is in contrast to non-targeting MWCNTs shown with HEK293 cells where bulk heating is required to confer cell ablation; altogether, we have shown that effective targeting of the MWCNTs now delivers highly efficient, highly localized cell ablation so much so as to avoid overall bulk heating (see below).

Optimization of in vitro cell ablation studies

Working concentration of α-PSMA–MWCNT conjugates. Next, the working concentration of MWCNT–antibody conjugate was determined by preparing a dose-response curve. Six concentrations of α-PSMA ranging from 0.5 to 12 μg were conjugated to MWCNTs, to determine a working concentration of antibody that could be effectively used for further ablation studies. Figure 3(a) shows the increased efficiency in ablation of LNCaP cells with increasing amounts of α-PSMA conjugated onto MWCNTs. Initially, a linear increase in cell ablation efficiency was observed at lower concentrations. However, when more than 5 μg of α-PSMA was conjugated onto the MWCNTs, the efficiency of cell ablation decreases and begins to plateau, with no significant difference between 10 and 12 μg of antibody addition. Although we have not

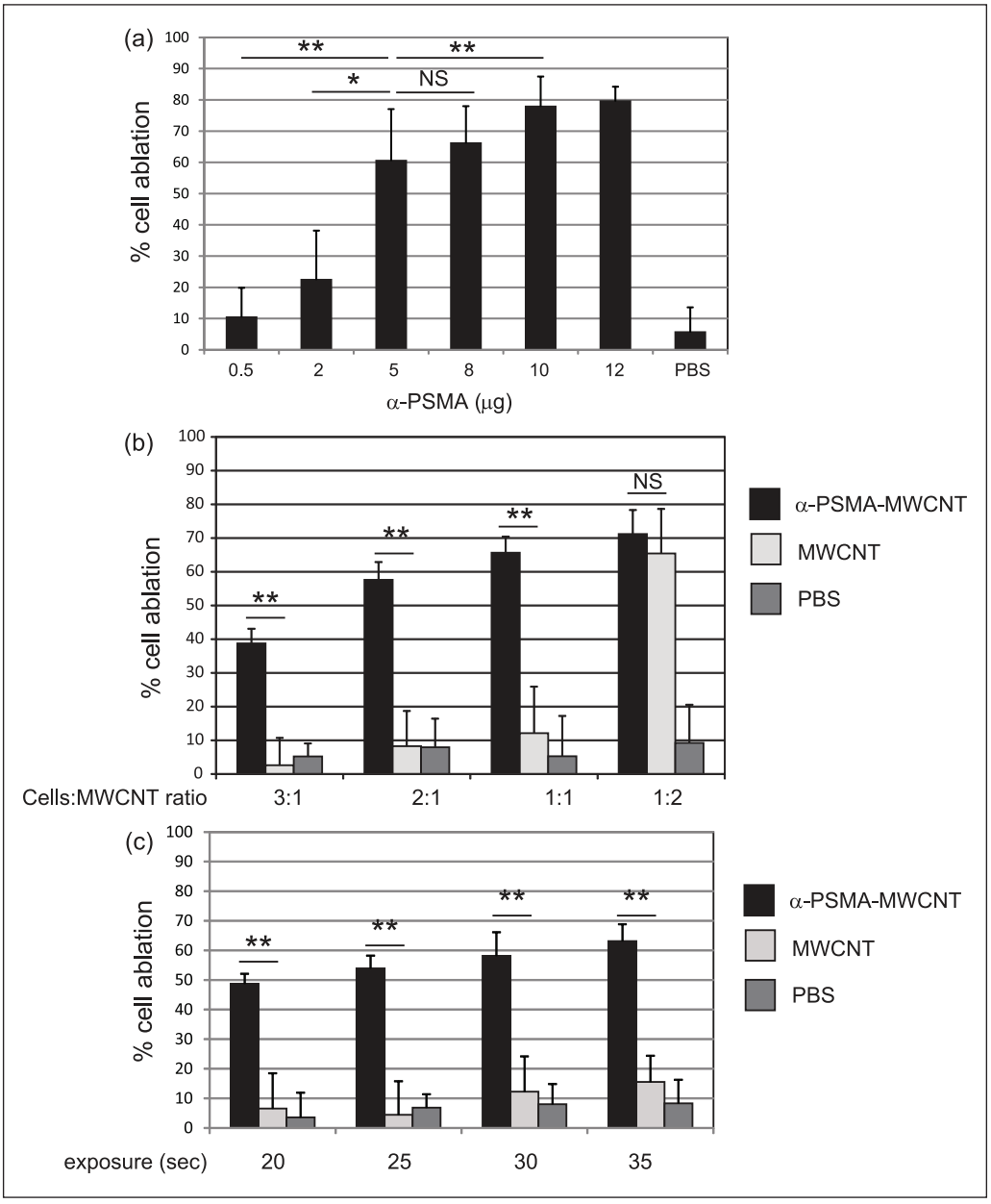

Figure 3. Optimizing targeted cell ablation of LNCaP cells. (a) Different amounts of α-PSMA were conjugated to MWCNTs and used for cell ablation studies (n = 5). (b) Different volumetric ratios of cells to α-PSMA–MWCNT conjugates were assessed in cell ablation studies. It could be observed that at the 1:2 ratio, the MWCNT alone results in significant amount of cell killing; this is due to the inability to wash away the large amounts of nanoparticles (n = 3). (c) Using the 2:1 ratio, cells–α-PSMA–MWCNT mixture was exposed to different lengths of time (n = 3). Statistical significance was determined between different concentrations (*$p < 0.05$; **$p < 0.005$; NS, not significant).

saturated the amount of antibody on the MWCNT (see Figure 2), it appears that between 8 and 10 μg of antibody in the conjugation reactions confers sufficient binding to the PSMA targets on LNCaP cells. This suggests that a critical content of antibody per MWCNT is required for optimal targeting, and the more antibody-laden MWCNTs do not lead to more particles per cell surface. For all further experiments, 5 μg of α-PSMA was conjugated to MWCNTs.

Determination of cell:MWCNT ratio. The ratio of LNCaP cells to α-PSMA–MWCNT conjugates was optimized by altering the ratio of cells to MWCNT conjugates. Four volumetric ratios of cells to α-PSMA–MWCNT conjugates (3:1, 2:1, 1:1, and 1:2 cell to conjugate) were examined, while other conditions were kept consistent. As the concentration of α-PSMA–MWCNT conjugates increased, higher cell ablation efficiency was observed (Figure 3(b)). When increased α-PSMA–MWCNT conjugates are incubated with LNCaP,

the cell ablation increases from 38.8%±4.3% at a 3:1 ratio of cells:MWCNT conjugates ($p=2.61\times10^{-9}$, α-PSMA–MWCNT vs MWCNT) to 71.2%±4.7% at 1:2 cells:MWCNT conjugates ($p=0.266$, α-PSMA–MWCNT vs MWCNT).

Unconjugated MWCNTs did not demonstrate any cell ablation potential; however, when a 1:3 ratio of cells: unconjugated MWCNT conjugates was used, we observed a significant increase in cell ablation. We observed a similar result in our previous assessment of α-TSHR–MWCNT targeting of papillary thyroid cancer cells.[20] The washing of high MWCNTs to cell mixture was insufficient to remove the excess concentration of nanoparticles, and enough residue MWCNTs remained to confer some cell ablation. Finally, we did not observe a significant difference in PBS controls, with 5%, 8%, 5%, and 9% cell loss in 3:1, 2:1, 1:1, and 1:2 cell to MWCNT mix, respectively, with laser exposure, suggesting that laser itself has no detrimental effects.

Length of exposure to laser. Finally, we evaluated the effects of laser exposure in cell ablation by lengthening the time of laser exposure. LNCaP cells incubated with α-PSMA–MWCNT were exposed to 2.7 W laser for different lengths of time (20, 25, 30, and 35 s; Figure 3(c)). Simultaneously, we also assessed unconjugated-MWCNT and PBS incubated with LNCaP as controls. With longer exposure, we observed an increase in cell ablation efficiency with α-PSMA–MWCNTs: 49% ($p=2.05\times10^{-8}$, α-PSMA–MWCNT vs MWCNT, at 20 s), 54% ($p=1.59\times10^{-9}$, α-PSMA–MWCNT vs MWCNT, at 25 s), 58% ($p=4.93\times10^{-8}$, α-PSMA–MWCNT vs MWCNT, at 30 s), and 63% (3.23×10^{-10}, α-PSMA–MWCNT vs MWCNT, at 35 s). No specific cell ablation was also observed with either unconjugated-MWCNT or PBS. Thus, PSMA target–bound MWCNTs exposed to laser for longer time periods result in higher cell ablation. When the temperature of the tube was monitored, we observed only small temperature changes between the different time points, with the highest bulk solution temperature observed was 41.2°C at 35 s.

Selective α-PSMA–MWCNT targeting of CaP cells

To evaluate whether α-PSMA–MWCNTs could exhibit specific PSMA-targeted cell ablation, we used PSMA-null PC3 cells (Figure 4(a)). In principle, each MWCNT molecule has multiple carboxylic groups that can serve as binding platforms for numerous moieties. Exploiting this property, we dual-functionalized MWCNTs with Cy5-PEG_{5000}-NH_2 and maleimide-PEG_{5000}-NH_2 (onto which α-PSMA was linked), thus allowing for selective fluorescent imaging of PSMA-targeted cells (Figure 4(b)). We also prepared negative untargeted single conjugated Cy5–MWCNT and PBS controls to demonstrate non-selective interactions to the cells (data not shown). As expected, the dual-labeled α-PSMA–Cy5–MWCNT conjugates only interacted with LNCaP and not PC3 cells. Finally, selective cell ablation of α-PSMA–MWCNT conjugates was evaluated between LNCaP and PC3 cells (Figure 4(c)). It was observed, and confirming, that only LNCaP cells were sensitive to α-PSMA–MWCNT with 63.0%±8.8% cell death, compared to 9.7%±7.2% with PSMA-null PC3 cells ($p=0.00011$).

α-PSMA–MWCNT targeting confers extreme nearfield cell ablation without bulk heating

Central to our approach of mediating extreme nearfield cell ablation, we assessed bulk temperature of the media during our ablation experiments. In Figure 1, we demonstrated non-targeted cell ablation of HEK293 cells; the temperature of the media in our non-targeted experiments resulted in complete cell death in 20-s laser exposure, where the bulk temperature reached up to 60°C in approximately 19 s (Figure 5(a)). Exposures of 5 and 10 s to the laser did not significantly increase the bulk temperature of the mixture, as the temperature was well below 50°C, the tolerable temperature threshold for normal cells.

We further assessed the bulk temperature of α-PSMA–MWCNT targeting of LNCaP cells (using 2:1 cells:MWCNT ratio) and found no significant increases in bulk temperature of the mixture (Figure 5(b)). Even after prolonged exposure of up to 90 s, which is well beyond our 30-s laser exposure of targeted ablation experimental design, the bulk temperature of the cell–α-PSMA–MWCNT mixture remained essentially unchanged due to the minimal remaining concentration of non-bound MWCNTs after multiple washes.

This supports our assertions of a nearfield targeted photothermal ablative strategy as being extremely effective without bulk heating, and represents a significant departure from current focal methodologies. Significant tumor cell killing without a bulk heating in the clinical setting would greatly minimize extracellular and tissue structure damage of patients.

Discussion

There are a number of obstacles with the current treatment options for CaP. Surgical removal of the tumor and/or the prostate itself, and radiotherapy including external beam radiation therapy (EBRT) and brachytherapies, are all limited to early, localized stages of CaP and are often associated with serious complications, including damage to surrounding tissues, erectile dysfunctions, and urinary incontinence.[31–33] Biological targeting using either hormone-directed anti-androgens or androgen deprivation and chemotherapies, while effective in earlier stages, eventually leads to therapeutic resistance. The process of drug resistance is a result of extensive genetic heterogeneity in advanced disease allowing for therapeutics to initiate selective pressures on the tumor cells, where cells will often

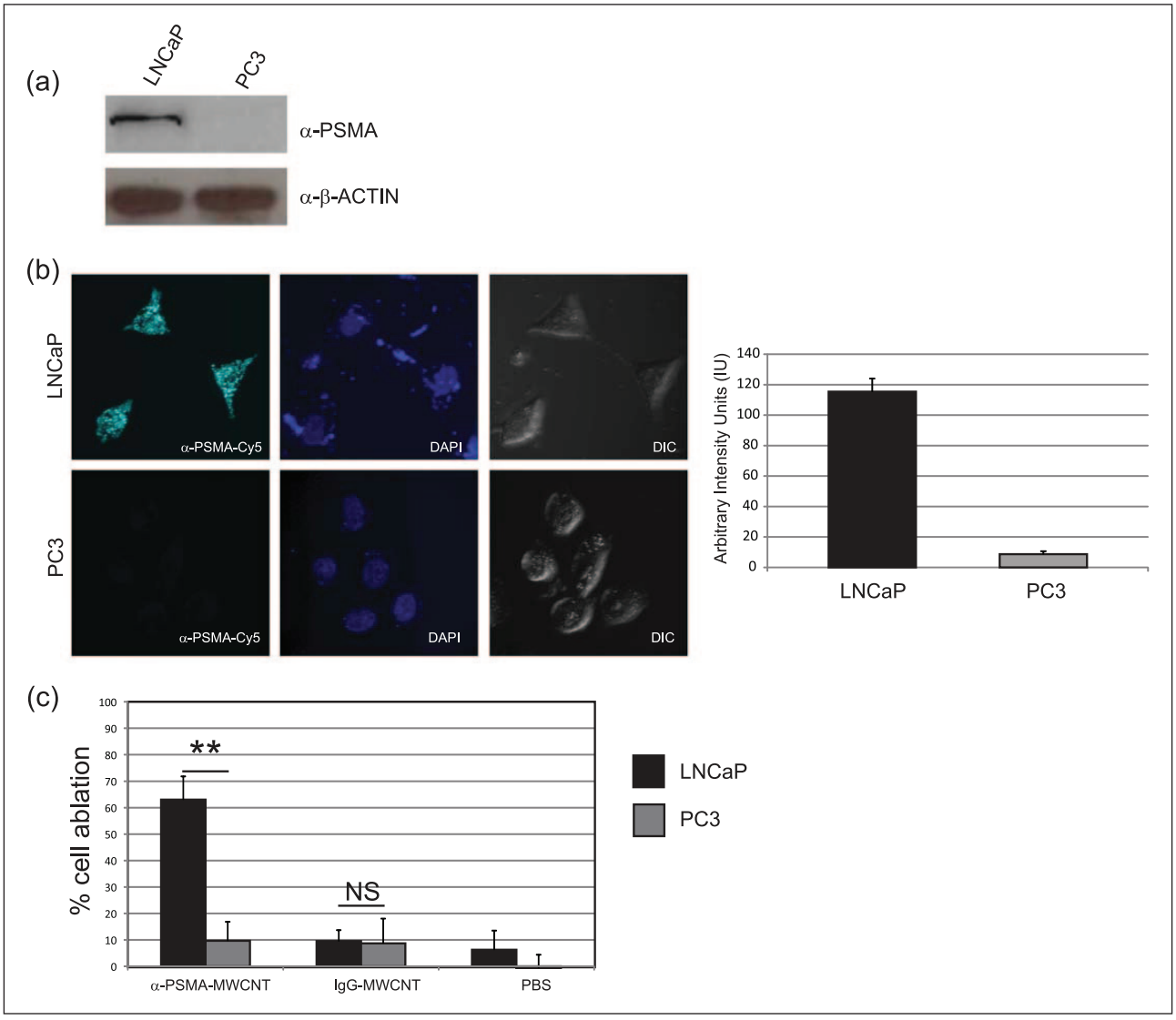

Figure 4. Selective PSMA targeting of LNCaP versus PC3 cells. (a) Western blot analysis of PSMA-positive LNCaP cells versus PSMA-negative PC3 prostate cancer cells. (b) Dual labeling of MWCNTs with α-PSMA and Cy5, for live imaging LNCaP and PC3 cells. Shown are stacked images from the spinning disk confocal microscope of LNCaP and PC3 cells labeled with Cy5, nuclear staining marker DAPI, and corresponding differential interference contrast (DIC) whole cell image. Intensity measurements were made for Cy5 staining using ImageJ software of numerous other slides and represented graphically next to the confocal images. A total of 20 cells were selected from images for which intensity analysis was performed. (c) Cell ablation experiments using α-PSMA–MWCNT against LNCaP and PC3 cells. IgG–MWCNT conjugates and PBS were used as controls in these studies (n = 5). Statistical significance was determined between the different concentrations (**$p < 0.005$; NS, not significant).

incur mutations to the target protein and hence the evolution into drug resistance tumors.[34] Therefore, there is a need for a novel and selective platform for circumventing some of the problems posed with traditional approaches regarding CaP treatment.

One of the methods to evade current genetic heterogeneity in CaP treatment is to promote physical damage on tumors via a photothermal approach, either in combination with surgery or by itself. Similar to radiotherapy, physical damages exerted by the photothermal bulk-heating approach are effective in ablating tumor cells in that they cause irreversible damage onto the tumor, as shown in Figure 1. Nevertheless, significant damages to nearby, non-targeted tissues and structures upon treatment still remain a major challenge. Furthermore, to achieve desired effects, different groups have reported either use of prolonged exposure time with laser, extreme high laser power, or an excessive amount of nanoparticles, making it a challenge for use in vivo and/or clinics.[18,19,35–37] We have comparatively summarized the use of a number of different nanoparticles in targeted and untargeted in vitro experiments in Supplemental Data S3.

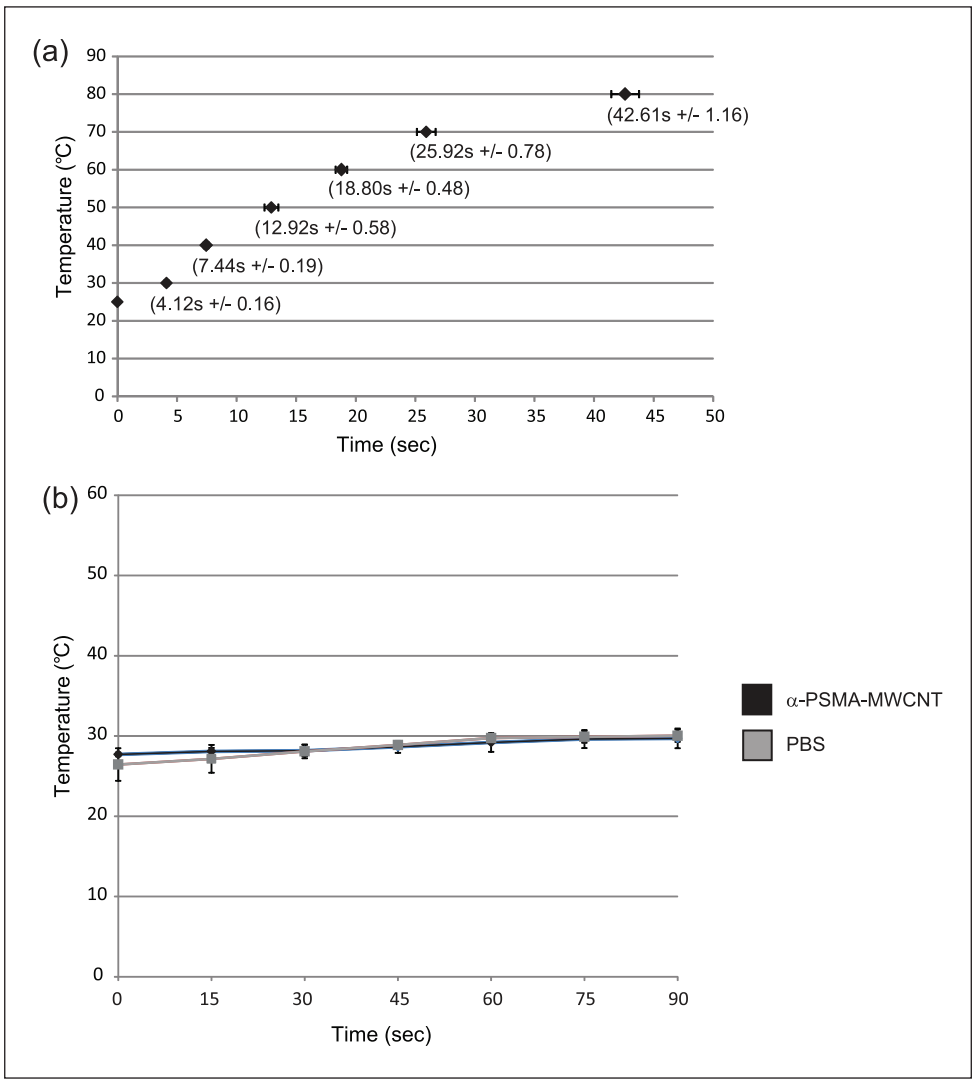

Figure 5. Bulk temperature analysis of cell–MWCNT mixtures. (a) Temperature rate readings of LNCaP cells mixed with PEG–MWCNTs (2:1 ratio; n = 3). Graph shows the time taken to reach fixed temperatures (30°C, 40°C, 50°C, 60°C, 70°C, and 80°C). (b) Temperature monitoring of α-PSMA–MWCNT targeting experiment of LNCaP cells, over 90 s. Temperature readings were also performed with PBS control experiments (n = 5).

To approach these difficulties, we have developed a targeted nanoparticle approach of using a tumor-specific targeting moiety conjugated to PEG-functionalized MWCNTs. Other groups have found significant non-specific binding of nanoparticles, due to lack of PEGylation (addition of polyethylene glycol), allowing for misguided non-targeted cell killing.[14,15,17,38–43] Almost all have not included a negative relevant control cell line to ensure specificity.[14–17,38,43–45] Therefore, by directing energy provided from laser sources to α-PSMA-conjugated PEG-functionalized MWCNTs placed in extreme proximity to the surface of tumor cells, we have demonstrated the capacity of this platform to exclusively damage and/or destroy targeted cells upon treatment without significant bulk heating. To achieve over 80% of targeted cell ablation (approximately 240,000 cells out of 300,000 cells), only 0.33 μg of functionalized MWCNTs, that would approximately equate to 100,000 particles per cell with cells expressing approximately 180,000 PSMA surface antigens,[46] was needed to be exposed by a 2.7-W laser for 30 s (Figure 4(a)) without a significant increase in medium bulk temperature. MWCNTs have two distinct characteristics that would allow the achievement of such significant cell ablation; first, the high thermal conductivity of the particles to generate high localized heat, and second, the motile force of the particles upon laser exposure into the cells, thereby causing significant cell damage.[47] In this regard, our nanoparticle targeted cell ablation method greatly outperforms currently available nanoparticle-mediated photothermal methods, opening up possibilities to be used for rapid and efficient tumor cell ablation with minimal damage to critical nearby tissue in effect displaying extreme nearfield efficacy. Currently

available nanoparticles, including carbon nanotubes, gold nanorods, nanospheres, and nanoshells, are potent enough to raise the temperature of the medium in a short period of time by magnitudes of tens of degrees via surface plasmon resonance when exposed to laser at their peak absorption range. Nevertheless, many of these models, even if they are targeted toward specific tumor mass, may face challenges in confining heat production at the very local levels; studies show that during the photothermal treatments of the cells using the nanoparticles, the temperature of the entire field is raised by a significant amount.[48–51] This could raise serious concerns about damage upon nearby, non-targeted tissue as the entire field is being affected. Our method tries to overcome this drawback by promoting target-specific attachment of the nanoparticle products to the tumor: This had led to dramatic reduction in overall heat generation of the field (Figure 5), while producing enough thermal energy at proximity to the target to induce sufficient damage on the tumor while minimizing temperature change. Moreover, almost all have not included a negative relevant control cell line to ensure specificity. Therefore, by directing energy provided from laser sources to α-PSMA-conjugated PEG-functionalized MWCNTs placed in extreme proximity to the surface of tumor cells, we have demonstrated the capacity of this platform to damage and/or destroy only targeted cells upon treatment without significant bulk heating.

Following the accomplishments of our in vitro cell ablation studies, an in vivo study is the next step in assessing the use of targeted MWCNTs in delivering nearfield photothermal damage to tumor lesions. Although a pre-clinical animal model would recapitulate some aspects of the extensive biological and anatomical nature of living organisms, there are some inherent challenges that would need to be addressed. First, unlike the in vitro experiments, in an in vivo environment, the tumor would be surrounded by a number of layers of cells which the stimulating laser light would need to penetrate to activate the tumor-targeted MWCNTs. However, previous studies have demonstrated that a continuous 1 W/cm^2 808-nm laser can penetrate up to 6.4 cm of bovine tissue samples.[52] Pulsing of the laser would achieve deeper penetration of the light. Moreover, the use of fiber optics can bring the light source in closer proximity to the tumor. Second, in vivo stability of the nanoparticle conjugate and the efficiency in biodistribution throughout the circulation would need to be evaluated. Our experiments have shown that an intraperitoneally injected untargeted fluoro-labeled antibody-conjugated MWCNT spreads throughout their body cavity with loss of signal within 72 h of injection (unpublished data). Localization and retention of the antibody-conjugated MWCNT to the directed tumor would next need to be evaluated. Finally, in vivo studies would also need to consider, but not limited to, cellular interactions, systemic reactions, and whole body metabolism and physiological responses.[53]

While we have extensively conjugated antibodies on the surface of MWCNTs for quantification and cell ablation purposes, in theory these nanoparticles may be used as a platform for any moiety, as long as the active groups on the moiety can be exploited by the conjugating chemistry. For example, we have dual-labeled the MWCNTs with a mixture of α-PSMA and Cy5 dye, which allowed us to visualize the actual localization of the nanoparticles on the targeted cell surface. Similarly, the potential for visualization of in vivo localization of dual-labeled MWCNTs cannot be ignored. Theoretically, with appropriate targeting system, this platform may be used to locate not only the primary tumor site but can also be used to identify metastatic or recurrent disease. Moreover, specifically addressing tumor heterogeneity, the possibilities can be considered that our platform has the ability to carry a multiple number of targeting molecules and pro-drugs to tumor cells. Coupling a pro-drug to the platform can limit systemic toxicities of current therapies.

Acknowledgements

P.J.R.R, E.J.M., M.P., and M.A.T. are inventors of the patent application (WO2015070351), BioNanofluid, for use as a contrast, imaging, disinfecting, and/or therapeutic agent.

Declaration of conflicting interests

The author(s) declared no potential conflicts of interest with respect to the research, authorship, and/or publication of this article.

Funding

This work was partially facilitated by grant from the Canadian Institute for Health Research—Proof of Principle—Phase I grant (PPP-139090).

References

1. Sadar MD, Hussain M and Bruchovsky N. Prostate cancer: molecular biology of early progression to androgen independence. *Endocr Relat Cancer* 1999; 6(4): 487–502.
2. Anderson K, Lutz C, van Delft, et al. Genetic variegation of clonal architecture and propagating cells in leukaemia. *Nature* 2011; 469(7330): 356–361.
3. Berger MF, Lawrence MS, Demichelis F, et al. The genomic complexity of primary human prostate cancer. *Nature* 2011; 470(7333): 214–220.
4. Lee W, Jiang Z, Liu J, et al. The mutation spectrum revealed by paired genome sequences from a lung cancer patient. *Nature* 2010; 465(7297): 473–477.
5. Pleasance ED, Cheetham RK, Stephens PJ, et al. A comprehensive catalogue of somatic mutations from a human cancer genome. *Nature* 2010; 463(7278): 191–196.
6. Puente XS, Pinyol M, Quesada V, et al. Whole-genome sequencing identifies recurrent mutations in chronic lymphocytic leukaemia. *Nature* 2011; 475(7354): 101–105.
7. Yu YP, Song C, Tseng G, et al. Genome abnormalities precede prostate cancer and predict clinical relapse. *Am J Pathol* 2012; 180(6): 2240–2248.
8. Baca SC and Garraway LA. The genomic landscape of prostate cancer. *Front Endocrinol* 2012; 3: 69.

9. Xu X, Zhu K, Liu F, et al. Identification of somatic mutations in human prostate cancer by RNA-Seq. *Gene* 2013; 519: 343–347.
10. Wu C, Wyatt AW, Lapuk AV, et al. Integrated genome and transcriptome sequencing identifies a novel form of hybrid and aggressive prostate cancer. *J Pathol* 2012; 227(1): 53–61.
11. Grasso CS, Wu YM, Robinson DR, et al. The mutational landscape of lethal castration-resistant prostate cancer. *Nature* 2012; 487(7406): 239–243.
12. Hieronymus H and Sawyers CL. Traversing the genomic landscape of prostate cancer from diagnosis to death. *Nat Genet* 2012; 44(6): 613–614.
13. Gelet A, Chapelon JY, Margonari J, et al. Prostatic tissue destruction by high-intensity focused ultrasound: experimentation on canine prostate. *J Endourol* 1993; 7(3): 249–253.
14. Hashida Y, Tanaka H, Zhou S, et al. Photothermal ablation of tumor cells using a single-walled carbon nanotube-peptide composite. *J Control Release* 2014; 173: 59–66.
15. Panchapakesan B, Lu S, Sivakumar K, et al. Single-wall carbon nanotube nanobomb agents for killing breast cancer cells. *NanoBiotechnology* 2005; 1: 133–139.
16. Burke A, Ding X, Singh R, et al. Long-term survival following a single treatment of kidney tumors with multiwalled carbon nanotubes and near-infrared radiation. *Proc Natl Acad Sci U S A* 2009; 106(31): 12897–12902.
17. Burlaka A, Lukin S, Prylutska S, et al. Hyperthermic effect of multi-walled carbon nanotubes stimulated with near infrared irradiation for anticancer therapy: in vitro studies. *Exp Oncol* 2010; 32(1): 48–50.
18. Avetisyan YA, Yakunin AN and Tuchin VV. Thermal energy transfer by plasmon-resonant composite nanoparticles at pulse laser irradiation. *Appl Opt* 2012; 51(10): C88–C94.
19. Pattani VP and Tunnell JW. Nanoparticle-mediated photothermal therapy: a comparative study of heating for different particle types. *Lasers Surg Med* 2012; 44(8): 675–684.
20. Dotan I, Roche PJ, Paliouras M, et al. Engineering multiwalled carbon nanotube therapeutic bionanofluids to selectively target papillary thyroid cancer cells. *PLoS ONE* 2016; 11(2): e0149723.
21. Huang YY and Terentjev EM. Dispersion of carbon nanotubes: mixing, sonication, stabilization, and composite properties. *Polymers* 2012; 4: 275–295.
22. Hashim U, Farehanim MAAN, Norhafiezah S, et al. Optical properties of MWCNTs dispersed in various solutions. In: *Proceedings of the 2nd international conference on biomedical engineering (ICoBE)*, Penang, Malaysia, 30–31 March 2015.
23. Chen CH, YJ Wu and Chen JJ. Gold nanotheranostics: photothermal therapy and imaging of Mucin 7 conjugated antibody nanoparticles for urothelial cancer. *Biomed Res Int* 2015; 2015: 813632.
24. Fekrazad R, Hakimiha N, Farokhi E, et al. Treatment of oral squamous cell carcinoma using anti-HER2 immunonanoshells. *Int J Nanomedicine* 2011; 6: 2749–2755.
25. Yang K, Yang G, Chen L, et al. FeS nanoplates as a multifunctional nano-theranostic for magnetic resonance imaging guided photothermal therapy. *Biomaterials* 2015; 38: 1–9.
26. Mhawech-Fauceglia P, Zhang S, Terracciano L, et al. Prostate-specific membrane antigen (PSMA) protein expression in normal and neoplastic tissues and its sensitivity and specificity in prostate adenocarcinoma: an immunohistochemical study using multiple tumour tissue microarray technique. *Histopathology* 2007; 50(4): 472–483.
27. Perner S, Hofer MD, Kim R, et al. Prostate-specific membrane antigen expression as a predictor of prostate cancer progression. *Hum Pathol* 2007; 38(5): 696–701.
28. Marchal C, Redondo M, Padilla M, et al. Expression of prostate specific membrane antigen (PSMA) in prostatic adenocarcinoma and prostatic intraepithelial neoplasia. *Histol Histopathol* 2004; 19(3): 715–718.
29. Sweat SD, Pacelli A, Murphy GP, et al. Prostate-specific membrane antigen expression is greatest in prostate adenocarcinoma and lymph node metastases. *Urology* 1998; 52(4): 637–640.
30. Anti-PSMA antibody [EPR6253] (ab133579), http://www.abcam.com/psma-antibody-epr6253-ab133579.html
31. Weyne E, Castiglione F, Van der Aa F, et al. Landmarks in erectile function recovery after radical prostatectomy. *Nat Rev Urol* 2015; 12(5): 289–297.
32. Incrocci L. Radiotherapy for prostate cancer and sexual health. *Transl Androl Urol* 2015; 4(2): 124–130.
33. Ficarra V, Novara G, Rosen RC, et al. Systematic review and meta-analysis of studies reporting urinary continence recovery after robot-assisted radical prostatectomy. *Eur Urol* 2012; 62(3): 405–417.
34. Chandrasekar T, Yang JC, Gao AC, et al. Mechanisms of resistance in castration-resistant prostate cancer (CRPC). *Transl Androl Urol* 2015; 4(3): 365–380.
35. Sun X, Zhang G, Patel D, et al. Targeted cancer therapy by immunoconjugated gold-gold sulfide nanoparticles using Protein G as a cofactor. *Ann Biomed Eng* 2012; 40(10): 2131–2139.
36. Yang TD, Choi W, Yoon TH, et al. Real-time phase-contrast imaging of photothermal treatment of head and neck squamous cell carcinoma: an in vitro study of macrophages as a vector for the delivery of gold nanoshells. *J Biomed Opt* 2012; 17(12): 128003.
37. Schwartz JA, Price RE, Gill-Sharp KL, et al. Selective nanoparticle-directed ablation of the canine prostate. *Lasers Surg Med* 2011; 43(3): 213–220.
38. Mendoza-Nava H, Ferro-Flores G, Ocampo-García B, et al. Laser heating of gold nanospheres functionalized with octreotide: in vitro effect on HeLa cell viability. *Photomed Laser Surg* 2013; 31(1): 17–22.
39. Chakravarty P, Marches R, Zimmerman NS, et al. Thermal ablation of tumor cells with antibody-functionalized single-walled carbon nanotubes. *Proc Natl Acad Sci U S A* 2008; 105(25): 8697–8702.
40. Marches R, Chakravarty P, Musselman IH, et al. Specific thermal ablation of tumor cells using single-walled carbon nanotubes targeted by covalently-coupled monoclonal antibodies. *Int J Cancer* 2009; 125(12): 2970–2977.
41. Xiao Y, Gao X, Taratula O, et al. Anti-HER2 IgY antibody-functionalized single-walled carbon nanotubes for detection and selective destruction of breast cancer cells. *BMC Cancer* 2009; 9: 351.

42. Lapotko D, Lukianova E, Potapnev M, et al. Method of laser activated nano-thermolysis for elimination of tumor cells. *Cancer Lett* 2006; 239(1): 36–45.
43. Melancon MP, Lu W, Yang Z, et al. In vitro and in vivo targeting of hollow gold nanoshells directed at epidermal growth factor receptor for photothermal ablation therapy. *Mol Cancer Ther* 2008; 7(6): 1730–1739.
44. Boca SC, Potara M, Gabudean AM, et al. Chitosan-coated triangular silver nanoparticles as a novel class of biocompatible, highly effective photothermal transducers for in vitro cancer cell therapy. *Cancer Lett* 2011; 311(2): 131–140.
45. Loo C, Lowery A, Halas N, et al. Immunotargeted nanoshells for integrated cancer imaging and therapy. *Nano Lett* 2005; 5(4): 709–711.
46. McDevitt MR, Barendswaard E, Ma D, et al. An alpha-particle emitting antibody ([213Bi]J591) for radioimmunotherapy of prostate cancer. *Cancer Res* 2000; 60(21): 6095–6100.
47. Heister E, Brunner EW, Dieckmann GR, et al. Are carbon nanotubes a natural solution? Applications in biology and medicine. *ACS Appl Mater Interfaces* 2013; 5(6): 1870–1891.
48. Qin Z, Wang Y, Randrianalisoa J, et al. Quantitative comparison of photothermal heat generation between gold nanospheres and nanorods. *Sci Rep* 2016; 6: 29836.
49. Huang HC, Rege K and Heys JJ. Spatiotemporal temperature distribution and cancer cell death in response to extracellular hyperthermia induced by gold nanorods. *ACS Nano* 2010; 4(5): 2892–2900.
50. Popp MK, Oubou I, Shepherd C, et al. Photothermal therapy using gold nanorods and near-infrared light in a murine melanoma model increases survival and decreases tumor volume. *J Nanomater* 2014; 2014: 450670.
51. Eldridge BN, Bernish BW, Fahrenholtz CD, et al. Photothermal therapy of glioblastoma multiforme using multiwalled carbon nanotubes optimized for diffusion in extracellular space. *ACS Biomater Sci Eng* 2016; 2(6): 963–976.
52. Hudson DE, Hudson DO, Wininger JM, et al. Penetration of laser light at 808 and 980 nm in bovine tissue samples. *Photomed Laser Surg* 2013; 31(4): 163–168.
53. Hartung T and Daston G. Are in vitro tests suitable for regulatory use? *Toxicol Sci* 2009; 111(2): 233–237.